Index

D

Color Plates

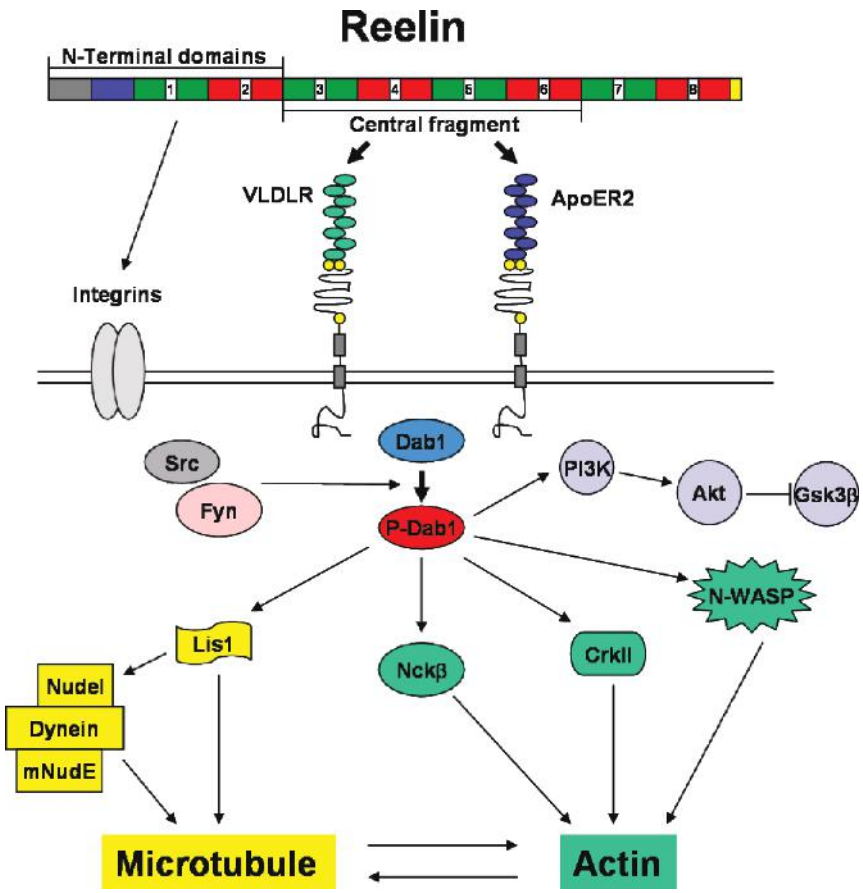

Fig. 1.1 The Reelin signaling pathway

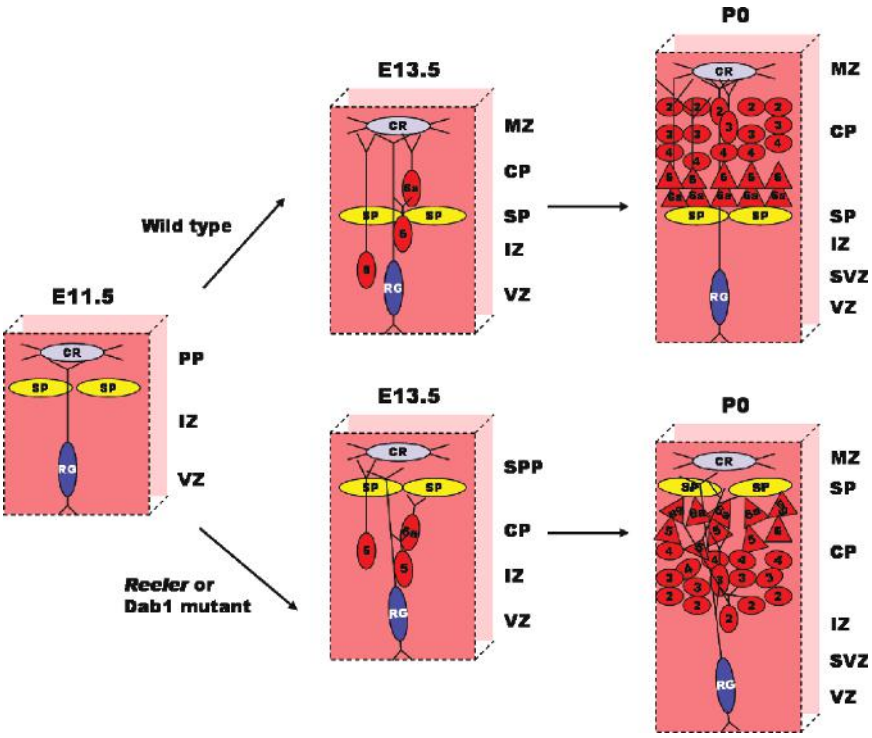

Fig. 1.2. Cortical development in normal and *reeler* and Dab1 mutant mice. In the embryonic cortex of normal mice, the preplate (PP) is split by the arrival of early radially migrating neurons, whereas in the *reeler* cortex, this does not happen and cells form a superplate structure (SPP). Cellular layers in the cortical plate (CP) are also disrupted in *reeler*. Other abbreviations: MZ, marginal zone; IZ, intermediate zone; VZ, ventricular zone; SVZ, subventricular zone; RG, radial glia; CR, Cajal-Retzius cells

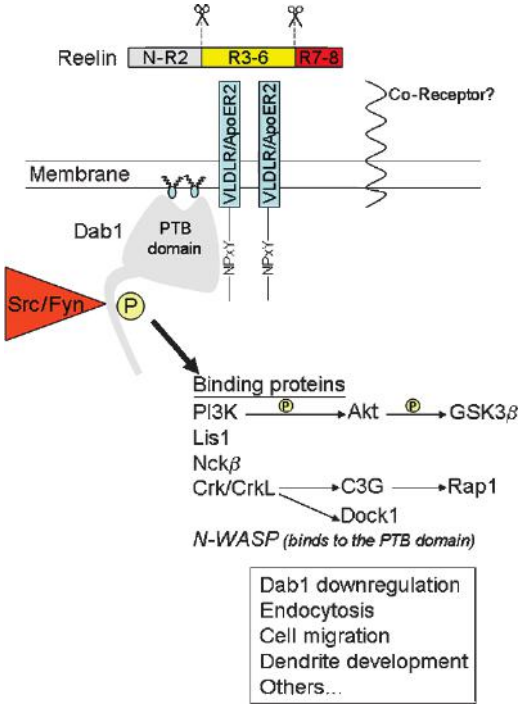

Fig. 3.1 Summary of the Reelin signaling pathway. See text for details

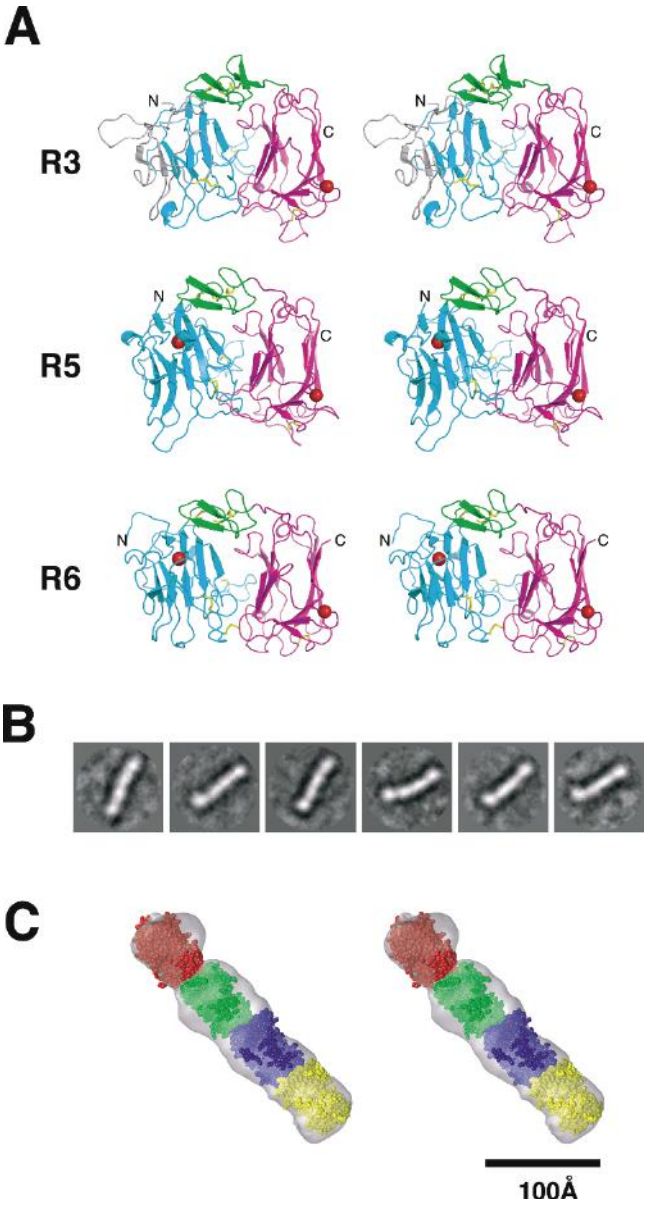

Fig. 5.2 Reelin repeat structure. (**A**) Crystal structures of single reelin repeat domains. Each panel shows a stereo presentation of R3 (top), R5 (middle), and R6 (bottom) structures. Subdomains are differently colored; subrepeat A (cyan), EGF (green), subrepeat B (magenta), and N- and C-termini are labeled. Bound calcium ions and disulfide bridges are shown as red spheres and yellow stick models, respectively. In R3, segments missing in the crystal structure are modeled and shown in gray. (**B**) Two-dimensional averages from representative particle classes obtained from the untilted electron micrographs of the R3–6 fragment. The width of each panel corresponds to 376 Å. (**C**) Three-dimensional volume map of an R3–6 fragment derived from single-particle tomography (gray) in a stereo representation. Four complete space-filling models for reelin repeats (R3, red; R4, green; R5, blue; and R6, yellow) are fitted into the envelope

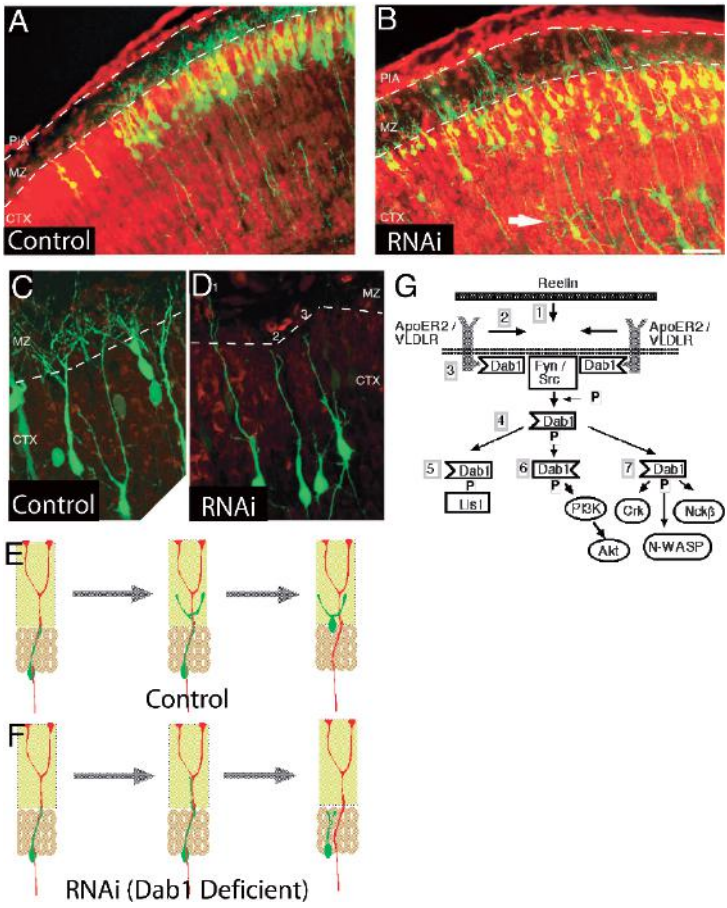

Fig. 7.1 Reelin Dab1 signaling in upper layer cortical neurons. (**A**, **B**) Low-magnification images of layer 2/3 cortical neurons on postnatal day 2 (P2), 7 days after *in utero* electroporation on E16 with either RNAi that suppresses Dab1 (RNAi) or control RNAi vector (Control). (**A**) Control electroporated neurons show precise lamination and exuberant dendritic growth in the MZ (dashed lines) on P2, whereas (**B**) Dab1-suppressed cells (RNAi) show disrupted lamination with occasional ectopic deep cells (arrow) and sparse dendrites in the MZ. (**C**, **D**) Higher-magnification images revealing extensive dendrites in (**C**) control cells and stunted dendrites in (**D**) RNAi-treated cells that either do not penetrate the MZ (cells 2 and 3) or stunted dendrites that do not show extensive secondary and tertiary branching in the MZ (cell 1). Scale bars: 50 μm (**A**, **B**); 20 μm (**D**). (**E**, **F**) Model of cell positioning and dendritogenesis in the developing cortex. (**E**) A control neuron (dark green) migrating on a radial glial process (red) extends a branched leading process into the MZ and then translocates through the upper ~50 μm of the CP, arresting migration at the first branch point of the leading process. (**F**) Dab1-deficient cells extend a leading process into the MZ but it remains simplified and the neuron does not translocate efficiently. (**G**) Dab1 interactions (after D'Arcangelo, 2006). Reelin secreted by CR cells (1) binds Reelin receptors (ApoER2 and VLDLR) in the migrating neuron causing (2) the clustering of Reelin receptors and Dab1. (3) The cytoplasmic clustering of Dab1 activates two SFKs (Fyn and Src) leading to (4) tyrosine phosphorylation of Dab1. (5) Phospho-Dab1 binds Lis1, a cytoplasmic dynein interacting protein encoded by *Lis1*, the gene underlying Miller-Dieker lissencephaly. (6) Phospho-Dab1 also activates PI3 kinase and Akt kinase and (7) binds adapter proteins Crk, Nckβ as well as N-WASP. Reelin signaling may regulate multiple cellular events including glial adhesion, somal positioning, and dendritogenesis. Panels **A–F** modified from Olson *et al*. (2006), copyright 2006 by the Society for Neuroscience

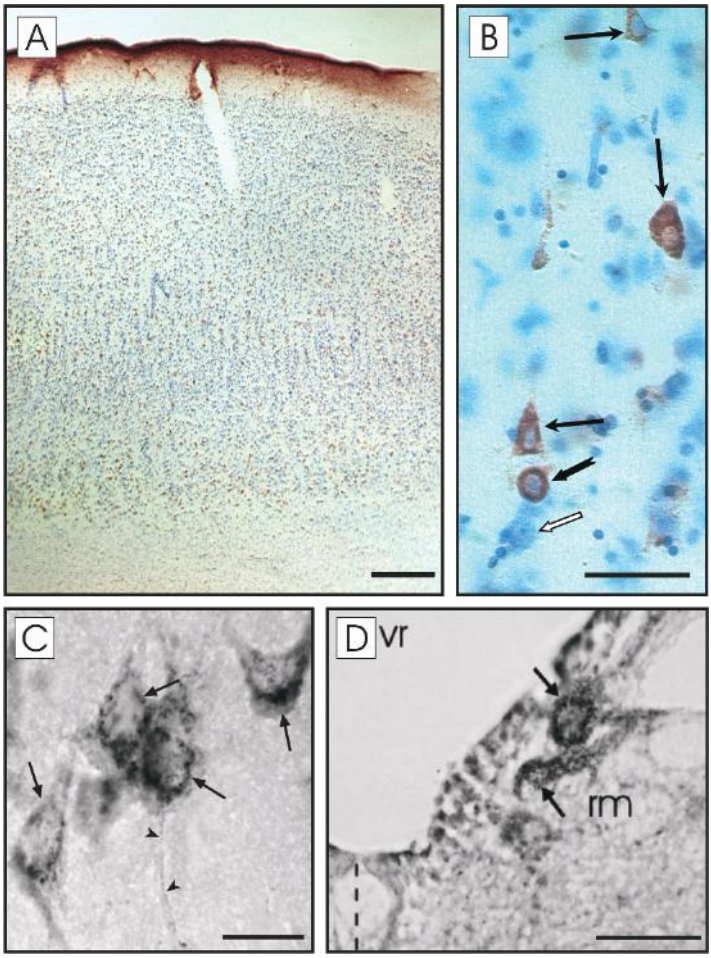

Fig. 8.1 Reelin-labeled neurons in the vertebrate brain. (**A**) Low magnification image of reelin labeling in the adult human cortex (BA39) demonstrating the abundant presence of reelin-labeled cells in all layers of the cortex (brown-stained cells). The section is counterstained with cresyl violet. (**B**) High magnification of the same cortical area as in **A** showing reelin-labeled pyramidal (plain black arrows) and nonpyramidal (notched arrow) cells. An unlabeled pyramidal cell is indicated with a white arrow. (**C**) Reelin-labeled cells of the adult rat entorhinal cortex. Arrows indicate the particle reelin labeling present in the cytoplasm, while arrowheads indicate reelin-labeled processes. (**D**) Reelin-labeled cells of the reticular rhombencephalic nucleus of the lamprey. Note the high similarity of the intracytoplasmic staining of these cells with the staining shown in **C**. vr, rhombencephalic ventricle; rm, nucleus reticularis medius. Scale bars: 500 µm (**A**); 50 µm (**B**); 15 µm (**C**); 150 µm (**D**). [**A**, **B** extracted from Roberts *et al*. (2005) *J. Comp. Neurol*. 482:294–308; **C** extracted from Perez-Costas (2002) Doctoral Thesis, p. 143; **D** extracted from Perez-Costas *et al*. (2004) *J. Chem. Neuroanat*. 27:7–21]

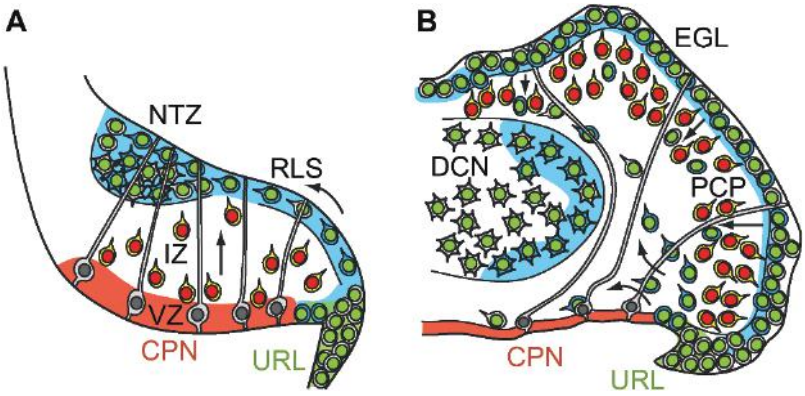

Fig. 10.1 Reelin signaling and cell migrations in cerebellar development. The diagrams show schematic views of the developing cerebellum in sagittal sections through the vermis, oriented with rostral to the left and dorsal to the top. (**A**) Early stage of cerebellar development (mouse E13.5). Cells derived from the upper rhombic lip (URL) (green nuclei) migrate nonradially (curved arrow) through the rostral rhombic lip migratory stream (RLS) to the nuclear transitory zone (NTZ). Reelin (blue) is expressed by many cells in the RLS and NTZ. At the same time, Purkinje cells (red nuclei) migrate radially (straight arrow) from the ventricular zone (VZ) of the cerebellar plate neuroepithelium (CPN) along radial glial cells (gray) through the intermediate zone (IZ), toward the RLS and NTZ. The Purkinje cells express cytoplasmic Dab1 (yellow). (**B**) Later stage of cerebellar development (mouse E17.5). The Purkinje cell plate (PCP) has formed, and the external granular layer (EGL) has replaced the RLS. Cells from the EGL migrate radially inward through the PCP (straight arrows), while unipolar brush cells migrate directly from the URL into the IZ (curved arrows). The deep cerebellar nuclei (DCN) contain neurons derived from the NTZ that have migrated radially inward toward the VZ

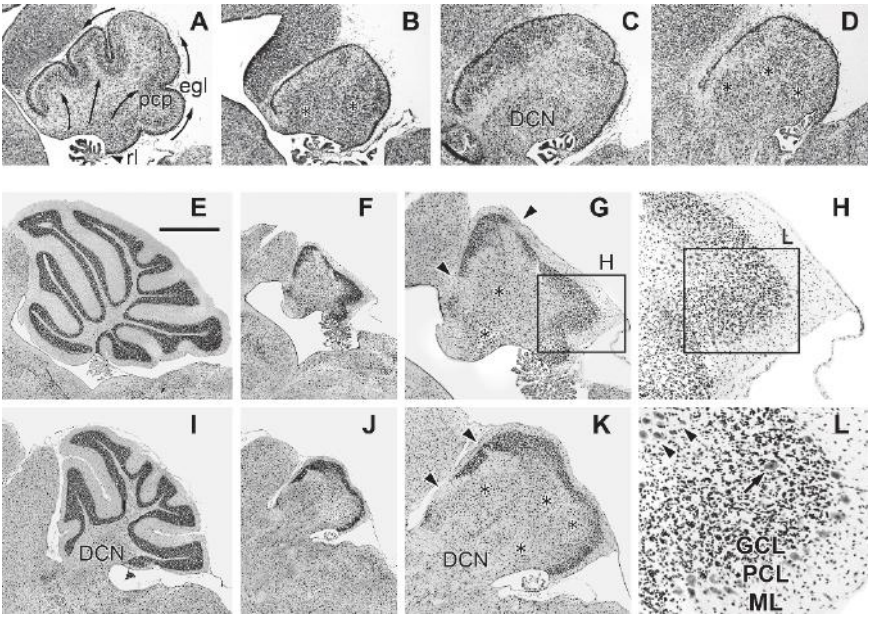

Fig. 10.2 Cerebellar histology in control and *reeler* mice. Sagittal sections through the cerebellar vermis (**A**, **B**, **E–H**, **L**) or hemisphere (**C**, **D**, **I–K**) of control and *reeler* (**B**, **D**, **F–H**, **J–L**) mice were stained with cresyl violet on P0.5 (**A–D**) or P22 (**E–L**). The boxed area in **G** is enlarged in **H**, and the boxed area in **H** is enlarged in **L**. In P0.5 controls, Purkinje cells had migrated to the Purkinje cell plate (pcp), and folia were developing by migration and proliferation of cells in the external granular layer (egl). In P0.5 *reeler* mice, the cerebellum was hypoplastic, no folia were developing, and Purkinje cells formed large, centrally located ectopic clusters (asterisks). The hypoplasia and defective foliation of the *reeler* cerebellum became even more obvious by P22. Most Purkinje cells in the P22 *reeler* cerebellum are located in the large central clusters, although some are isolated ectopically in the granule cell layer (GCL), and others form a nearly normal Purkinje cell layer (PCL) below the molecular layer (ML). In **L**, arrowheads indicate Purkinje cells in deep ectopia, and the arrow indicates a Purkinje cell in the GCL. The GCL in *reeler* consistently shows gaps (arrowheads in **G**, **K**), which may be related to the presumptive locations of fissures (Goldowitz *et al*., 1997). The deep cerebellar nuclei (DCN) in *reeler* are located near the normal location, but somewhat distorted by the Purkinje cell ectopia (Goffinet, 1983; Goffinet *et al*., 1984). Sections oriented as described for Figure 1. Scale bar (in **E**): **A–D**, 400 µm; **E**, **F**, **I**, **J**, 1000 µm; **G**, **K**, 500 µm; **H**, 200 µm; **L**, 100 µm

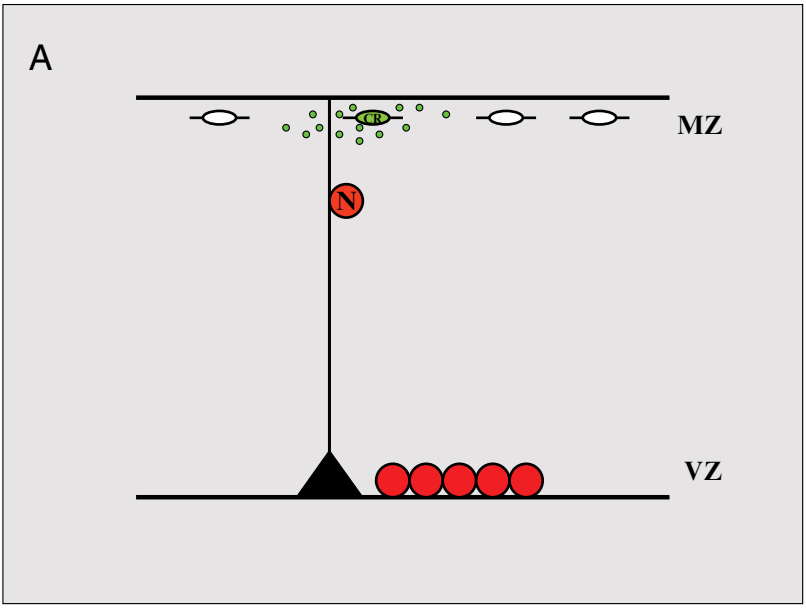

Fig. 11.1 (**A**) Schematic view of the developing cortex. A radial glial cell (black) is shown, extending a radial process from its perikaryon in the ventricular zone (VZ) toward the marginal zone (MZ). Neurons (red) in the ventricular zone are generated by asymmetric division of radial glial cells. A newly generated neuron (N) migrates along the radial glial process toward the marginal zone. Cajal-Retzius cells (CR; green) located in the marginal zone, secrete the glycoprotein Reelin (green dots) into the extracellular matrix. Reelin controls the positioning of radially migrating neurons by acting on both radial glial cells and migrating neurons

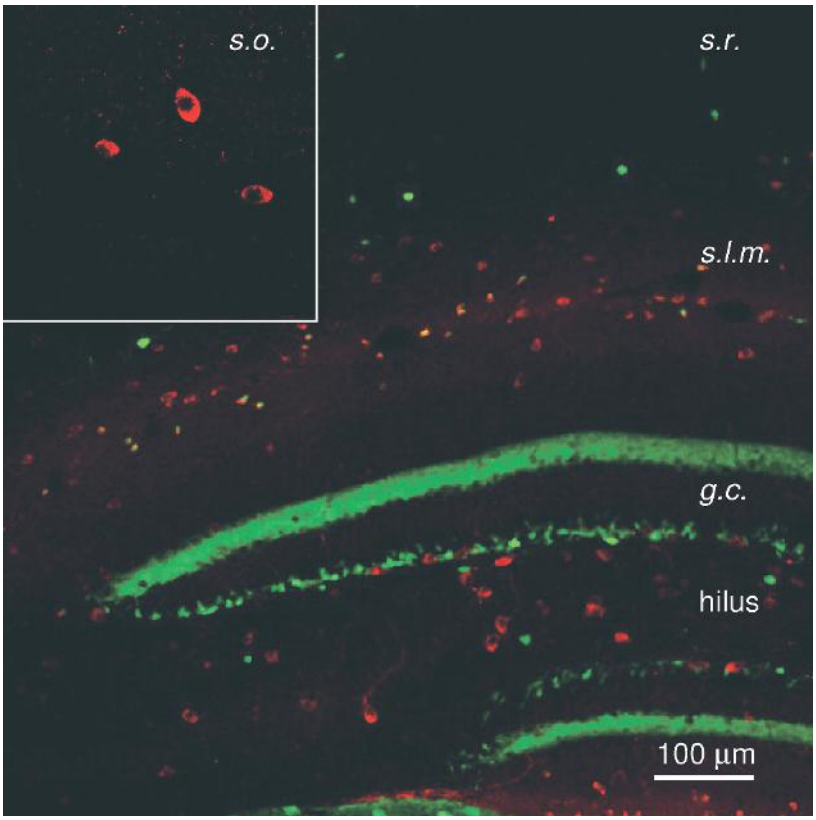

Fig. 12.1 Reelin-expressing cells in adult mouse hippocampus. Double immunofluorescent staining of a hippocampus cryosection obtained from a 6-week-old wild-type mouse. Note that Reelin-containing cells (red) were primarily distributed in the dentate hilar region (hilus) and stratum lacunosum-moleculare (*s.l.m.*) but also can be found in stratum oriens (*s.o.*) and stratum radiatum (*s.r.*) of CA1 region. Immunostaining of the calcium-binding protein calretinin (green) was used to visualize the dentate gyrus layers

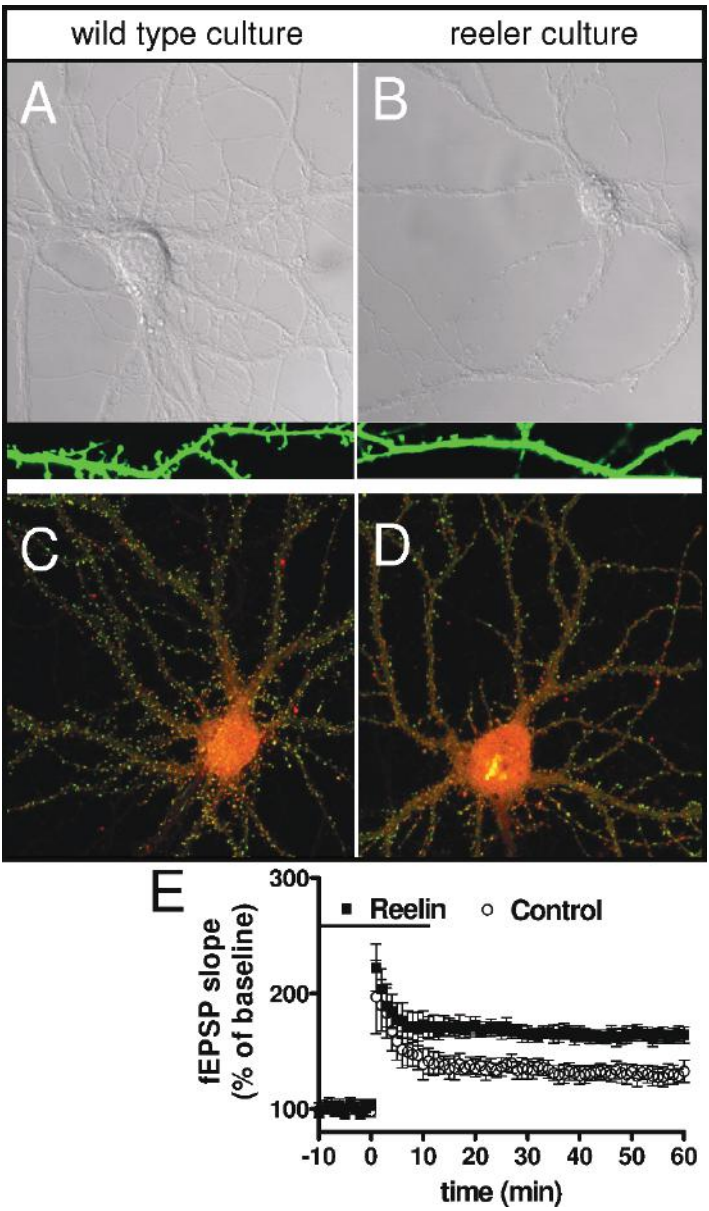

Fig. 12.2 Reelin signaling enhances glutamatergic function in the hippocampus. (**A**, **B**) In cultured embryonic mouse hippocampal neurons derived from homozygous Reeler embryos, stunted neurite growth and fewer neurite ramifications are seen; in addition, when neurons were filled with fluorophores to reveal dendritic spines, it was observed that neurons from wild-type cultures show significantly more spines in their primary dendrites. (**C**, **D**) Neurons from both wild-type and Reeler embryos are cultured for 2 weeks and then immunostained with NMDA receptor subunit NR1 and AMPA receptor subunit (GluR1) antibodies. A larger number of puncta that are positive for both NR1 and GluR1 were observed in wild-type cultures compared with Reeler cultures. (**E**) Long-term potentiation experiments using acute hippocampal slices prepared from 6-week-old mice. A 20-min perfusion of Reelin dramatically elevated the magnitude of tetanus-induced LTP

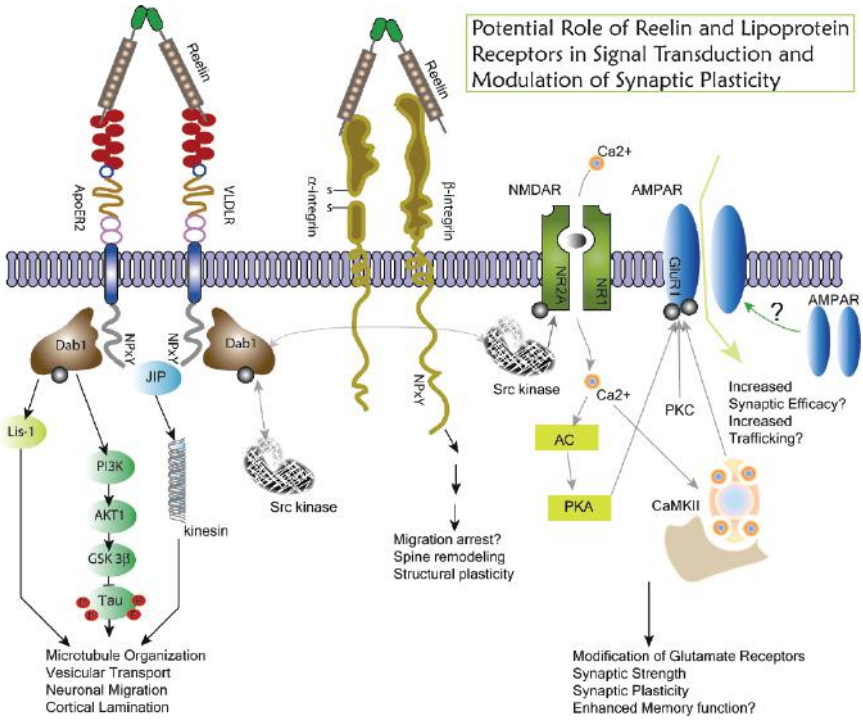

Fig. 12.3 Schematic representation of Reelin signaling and the subsequent enhancement of synaptic function in the adult hippocampus. Reelin binds and activates ApoER2/VLDLR and leads to tyrosine phosphorylation and activation of Dab1 and Src family protein tyrosine kinases. Src kinases phosphorylate NMDA receptor subunits and lead to enhanced channel conductance, augmented Ca^{2+} influx during activation, and increased synaptic plasticity. This increased synaptic plasticity may involve changes of AMPA receptor phosphorylation and trafficking as well. In response to Reelin signaling, PI3K and PKB/AKT can be activated as well, resulting in inhibition of tau phosphorylation. In addition to ApoER2/VLDLR, Reelin also activates integrins

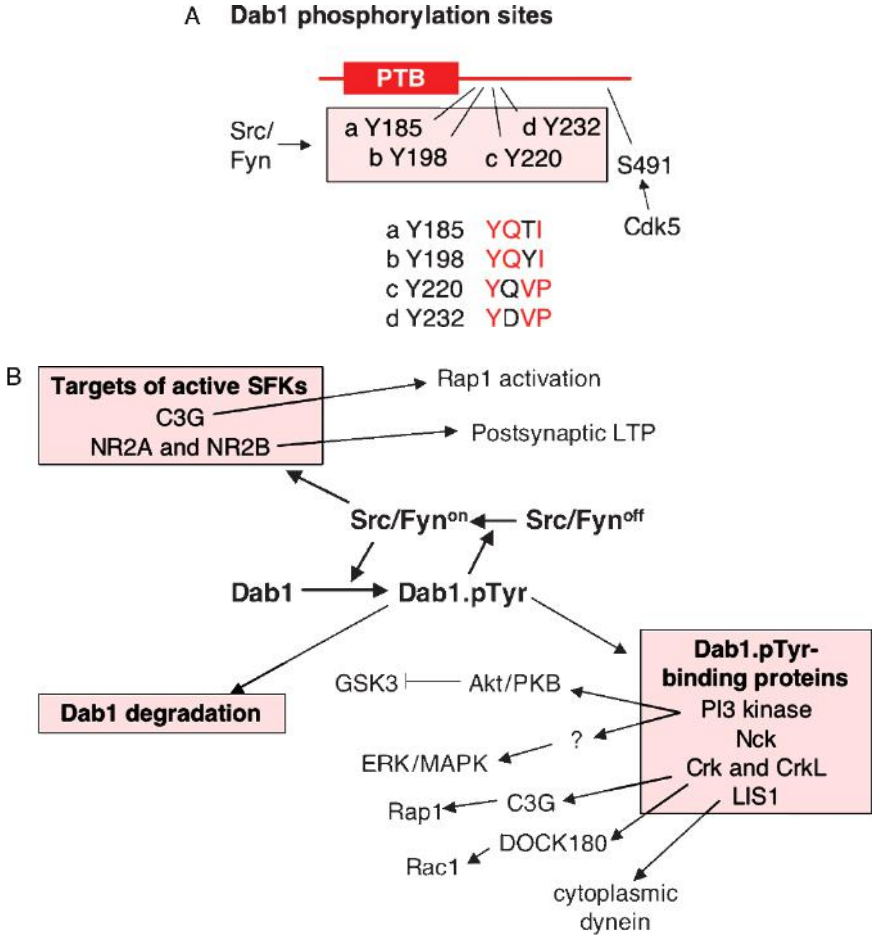

Fig. 13.2 Events downstream of Dab1 phosphorylation and SFK activation. (**A**) Phosphorylation sites in Dab1 that are phosphorylated by SFKs and Cdk5. (**B**) Events that may be important in Reelin signaling are shown separated into two categories: those triggered by active SFKs and those dependent directly on Dab1 phosphorylation

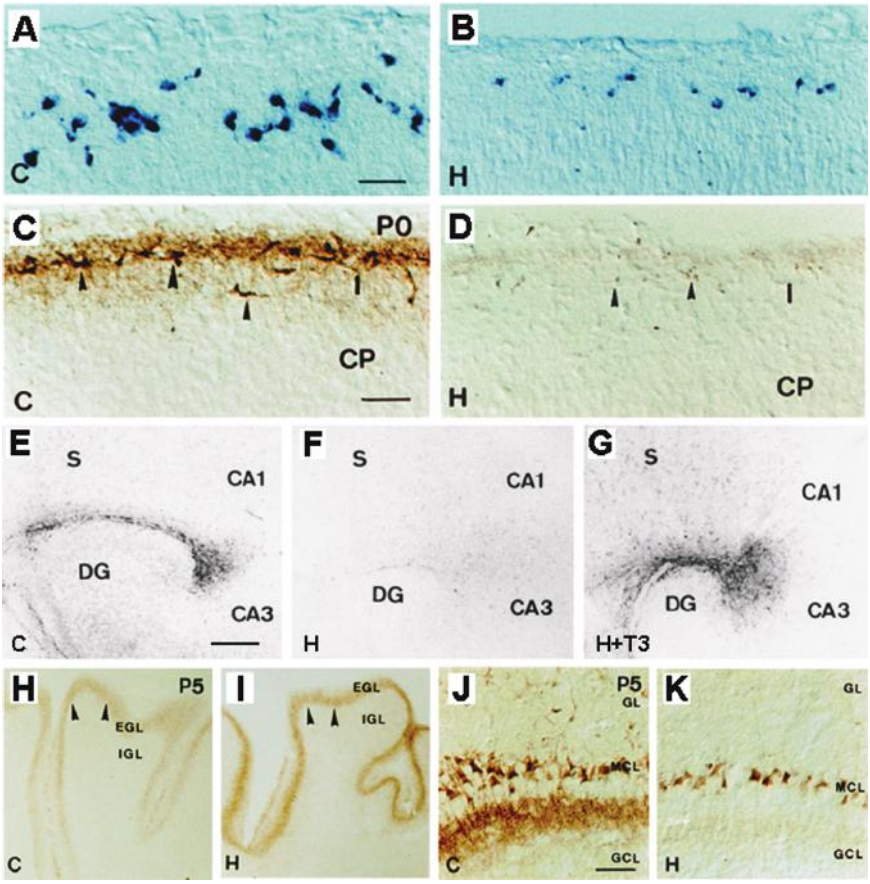

Fig. 15.1 Effects of hypothyroidism on *reelin* RNA and protein expression in the neonatal brain. (**A, B**) Pattern of *reelin* RNA expression in the neocortex of control (**A**) and hypothyroid (**B**) rats at P0. (**C, D**) Photomicrographs showing the distribution of CR50 antibody immunostaining in layer I of control (**C**) and hypothyroid rats (**D**) at P0. Some CR50-positive Cajal-Retzius cells are indicated by arrowheads. Note the decreased staining in hypothyroid animals. Cortical layers are indicated to the right. (**E–G**) Reelin expression detected by CR50 immunostaining in hippocampal organotypic slice cultures. (**E**) Slice from euthyroid rats incubated for 6 days in standard serum. (**F**) Slice from hypothyroid rats incubated for 6 days in thyroid-depleted serum. (**G**) Slices from hypothyroid rats incubated for 6 days in T3/T4-depleted serum supplemented with 500 nM T3. Note that the reduced expression levels in hypothyroid slices are rescued by T3 treatment. (**H–K**) Patterns of Reelin distribution in the cerebellum (**H**, **I**) and olfactory bulb (**J**, **K**) of control (**H**, **J**) and hypothyroid (**I**, **K**) rats at P5. Note the increased Reelin levels in the hypothyroid cerebellum and the opposite in the olfactory bulb. Abbreviations: C, control; CA3, CA1, hippocampal subdivisions CA3 and CA1; CP, cortical plate; DG, dentate gyrus; EGL, external granule cell layer; GCL, granule cell layer; GL, glomerular cell layer; H, hypothyroid; I, cortical layer I; IGL, internal granule cell layer; MCL, mitral cell layer; ML, molecular layer; S, stratum lacunosum-moleculare. Scale bars: **A**, 40 µm (applies to **A–D**); **E**, 200 µm (applies to **E–I**); **J**, 50 µm (applies to **J** and **K**). (Figure modified from Álvarez-Dolado *et al*., 1999. © *The Journal of Neuroscience*)

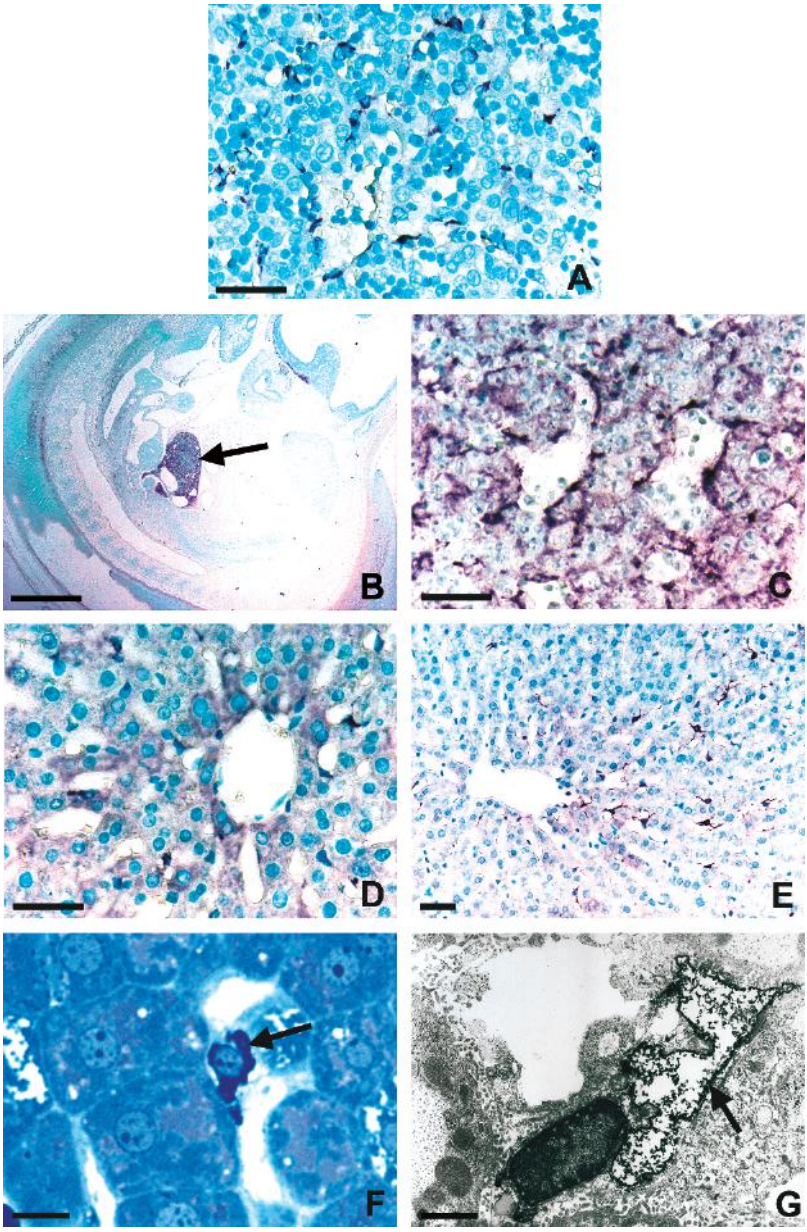

Figure. 17.1. Reelin (**A–D**, **F**, **G**) and GFAP (**E**) expression in human (**A**) and rat (**B–G**) liver. (A) Reelin immunostaining in stellate cells of human fetus at GW7. (B) Reelin immunostaining in liver of rat fetus at E13 (arrow). (C) Reelin immunostaining in stellate cells of rat fetus at E13; **C** is a high magnification of **B**. (D) Reelin immunostaining in adult rat stellate cells. (E) GFAP immunostaining in adult rat stellate cells. (F) Reelin immunostaining in a stellate cell of adult rat observed on a semithin section stained with toluidine blue (arrow). (G) Reelin immunostaining in a stellate cell of adult rat: electron microscopic examination; staining is observed in rough endoplasmic reticulum (arrow). Scale bars = 40 µm (**A**, **C–E**), 800 µm (**B**), 10 µm (**F**), and 2 µm (**G**)

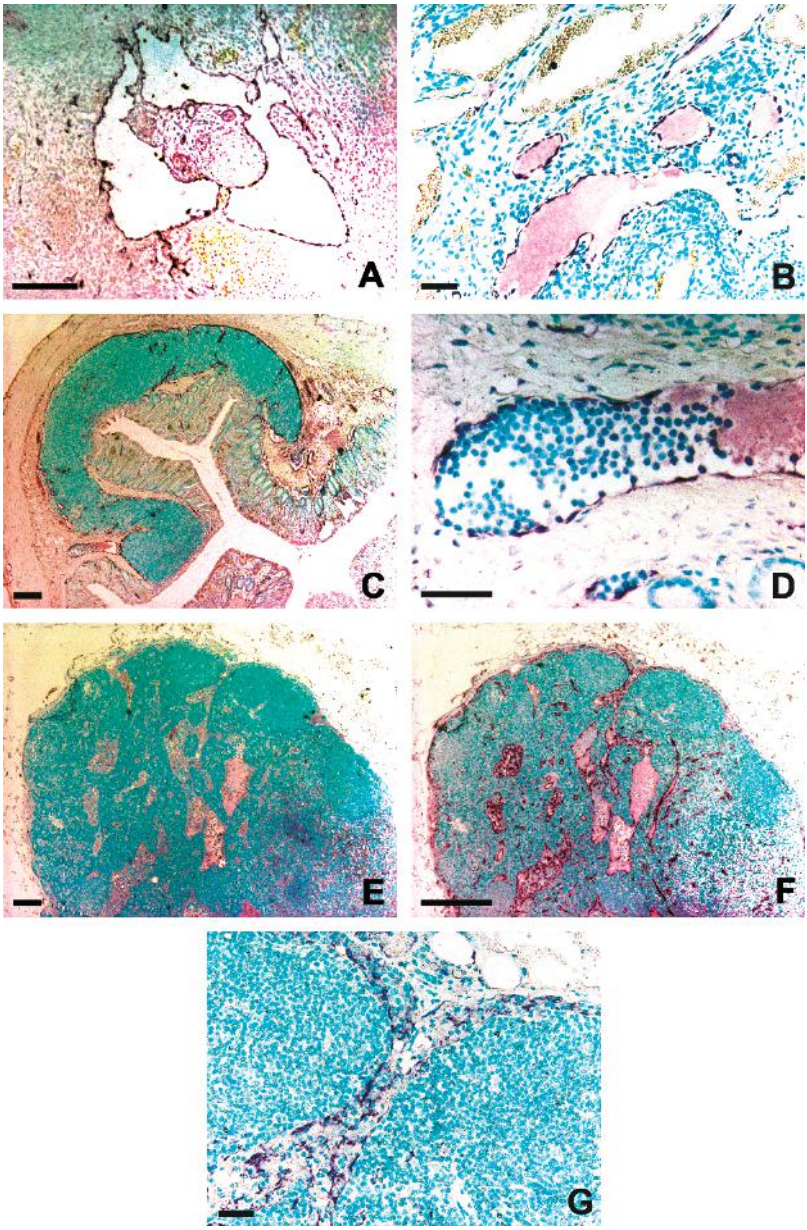

Figure 17.2 Reelin (**A–E**) and CD31 (**F**, **G**) expression in rat fetus (**A**), adult rat (**B–D**), and adult human (**E–G**). (A) Reelin immunostaining in the jugular lymphatic sac of rat fetus at E13. (B) Reelin immunostaining in lymphatics of adult rat ovarian medulla. **(C, D)** Reelin immunostaining of lymphatics around Peyer's patches in adult rat gut; **D** is a high magnification of **C**. **(E)**Absence of reelin immunostaining in adult human lymph node. **(F, G)** CD31 immunostaining in adult human lymph node; **G** is a high magnification of **F**. Scale bars = 150 μm (**A**, **C**, **E**) and 40 μm (**B**, **D**, **F, G**)

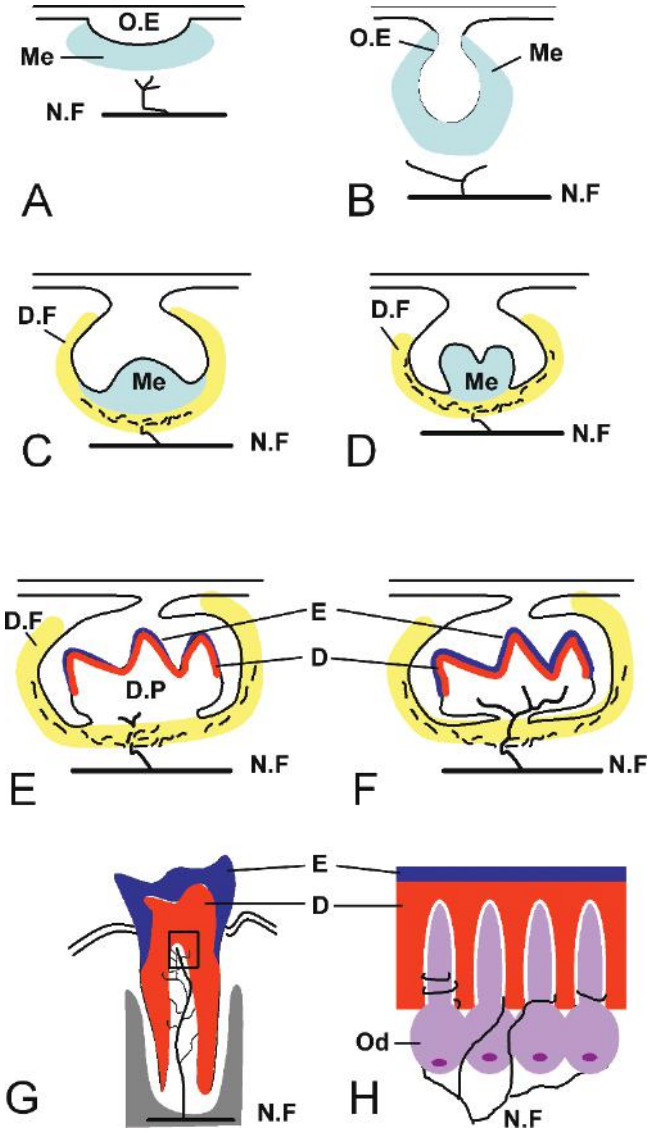

Fig. 19.1 Schematic representation of dental innervation during tooth development from embryonic stages **(A—D)** to postnatal stages **(E—H). (A)** Epithelial thickening stage. A plexus of nerve fibers is observed in the mesenchyme beneath the thickened oral epithelium. (**B**) Bud stage. The oral epithelium thickens and the mesenchyme undergoes a condensation. Axon sprouts grow toward the mesenchyme and continue to the epithelium as lingual and buccal branches. (**C**) Cap stage. Local axons form a plexus at the base of the primitive dental papilla and come into contact with the dental follicle. (**D**) Early bell stage. The number of axons increases in the dental follicle. (**E**) Late bell stage. At the onset of amelogenesis and dentinogenesis, the first sensory axons enter the dental papilla. (**F**) During early root formation, the number of pulpal axons increases. (**G**) During tooth eruption and with the advancing root formation, a rapid development of sensory pulpal axons leads to the formation of the subodontoblastic plexus of Raschkow. (**H**) Enlarged schematic representation of the dentin pulp complex innervation. The sensory nerve endings originating from the plexus of Raschkow coil around the cell bodies and processes of odontoblasts in the dentinal tubules. D, dentin; D.F, dental follicle; D.P, dental papilla; E, enamel; Me, mesenchyme; N.F, nerve fiber; Od, odontoblasts; O.E, oral epithelium

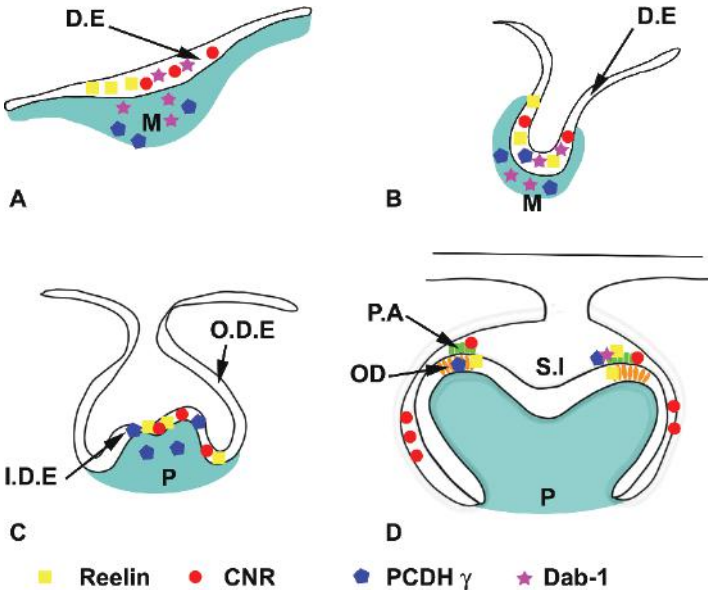

Fig. 19.2 Schematic representation of reelin gene expression and its receptors during successive stages of odontogenesis. Reelin is first detected in the oral epithelium from the initiation stage through the early bell stage. Then, reelin expression shifts in differentiating odontoblasts at the late bell stage. Dab1 is mainly expressed in both oral epithelium and dental mesenchyme during the initiation stages (epithelial thickening and bud stages). CNRs are present in the epithelium through the tooth development whereas PCDH-γ is expressed in both epithelial and mesenchymal compartments. D.E, dental epithelium; I.D.E, inner dental epithelium; M, mesenchyme, OD, odontoblasts; O.D.E, outer dental epithelium; P, dental papilla; P.A, preameloblasts; S.I, stratum intermedium

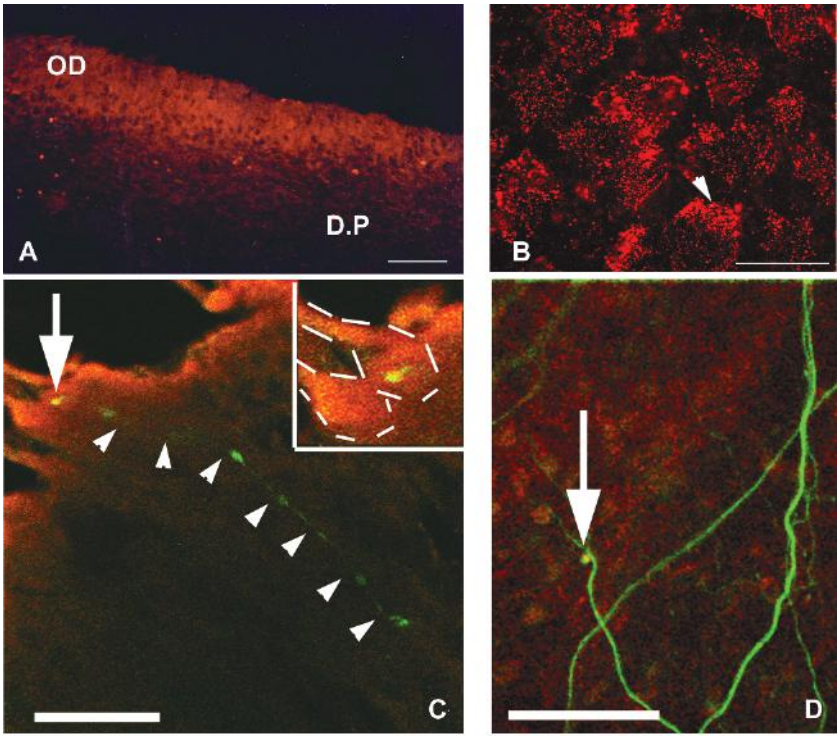

Fig. 19.3 Expression of reelin in human odontoblasts. (**A**) An immunolabeling of reelin performed with anti-reelin antibody 142 shows a signal in the odontoblast layer (OD). No staining is observed in dental pulp cells (D.P) (bar is 100 µm). (**B**) Immunofluorescence labeling with the same antibody, and without permeabilization of the cells, appears as reelin-positive patches localized around the cultured odontoblast cell membrane (arrowhead) (bar is 100 µm). (**C**) A double immunostaining with the monoclonal anti-reelin antibody and a polyclonal anti-neurofilament H on a human dental pulp section was analyzed by confocal microscopy. The nerve fiber course in the pulp can be followed (arrowheads). A yellow patch observed in a nerve varicosity, indicates a colocalization between nerve fiber and reelin close to the odontoblast membrane (arrow and insert) (bar is 20 µm). (**D**) Coculture of human odontoblasts and rat trigeminal ganglion shows the same colocalization (yellow) of reelin (red) and the varicosity (green) in the odontoblast cell layer (bar is 20 µm). [Modified from Maurin *et al*. (2004). Expression and localization of reelin in human odontoblasts. *Matrix Biol*. 23:277–285, with permission from Elsevier]

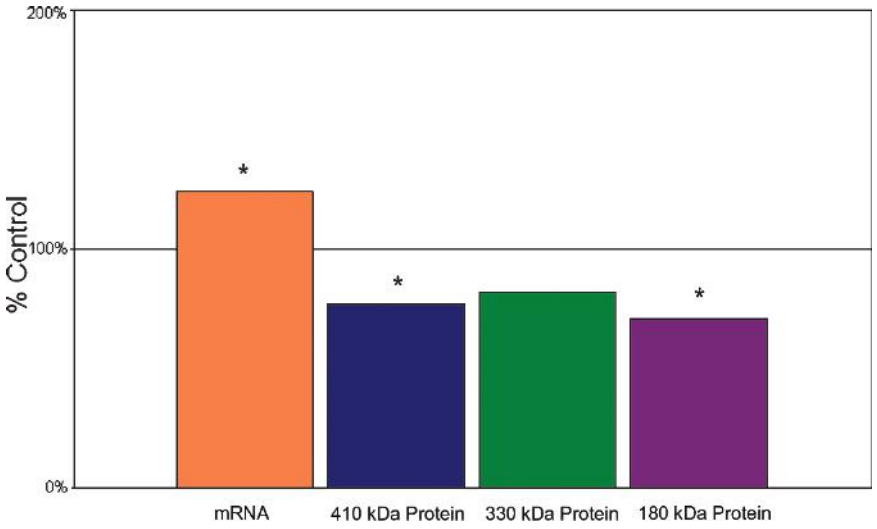

Fig. 22.2 The impact of clozapine on rat brain levels of Reelin. In clozapine-treated rat FC, Reelin protein showed significant downregulation of the 410- and 180-kDa isoforms while Reln mRNA was significantly upregulated versus controls

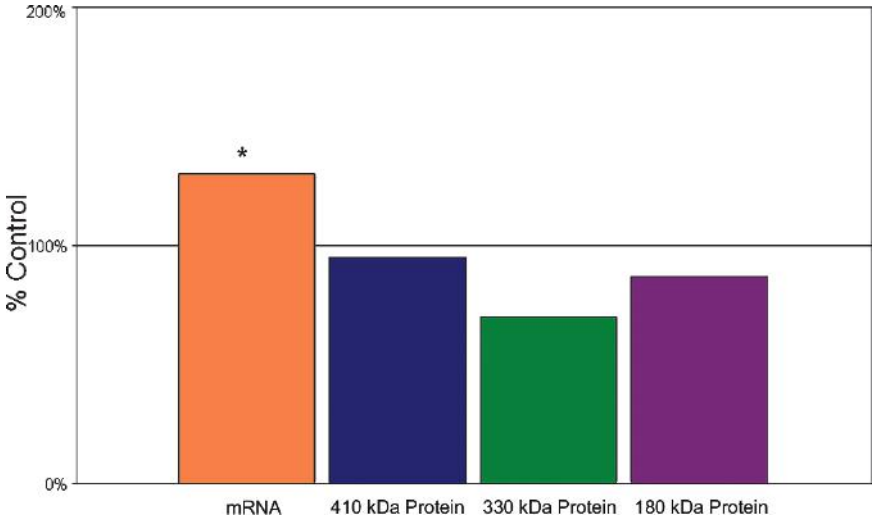

Fig. 22.3 The impact of fluoxetine on rat brain levels of Reelin. Reln mRNA was significantly upregulated in fluoxetine-treated rat FC versus controls

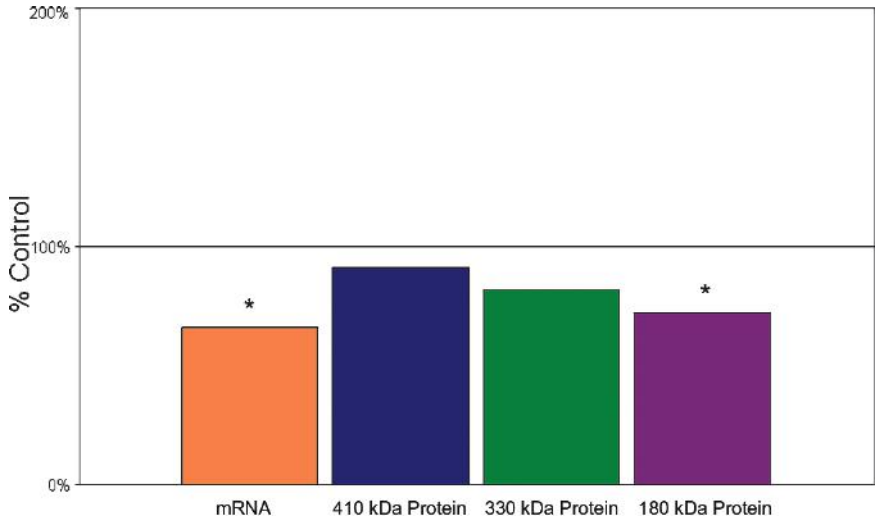

Fig. 22.4 The impact of haloperidol on rat brain levels of Reelin. Reelin protein showed the 180-kDa isoform was significantly downregulated as was Reln mRNA level in haloperidol versus control rat FC

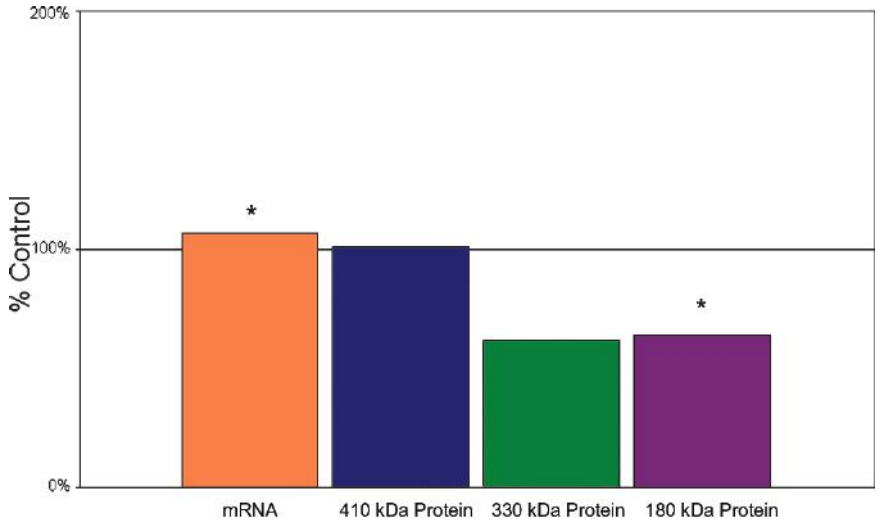

Fig. 22.5 The impact of lithium on rat brain levels of Reelin. The 180-kDa isoform of Reelin was significantly downregulated following chronic treatment with lithium. In contrast, Reln mRNA was significantly upregulated in lithium versus control rat FC

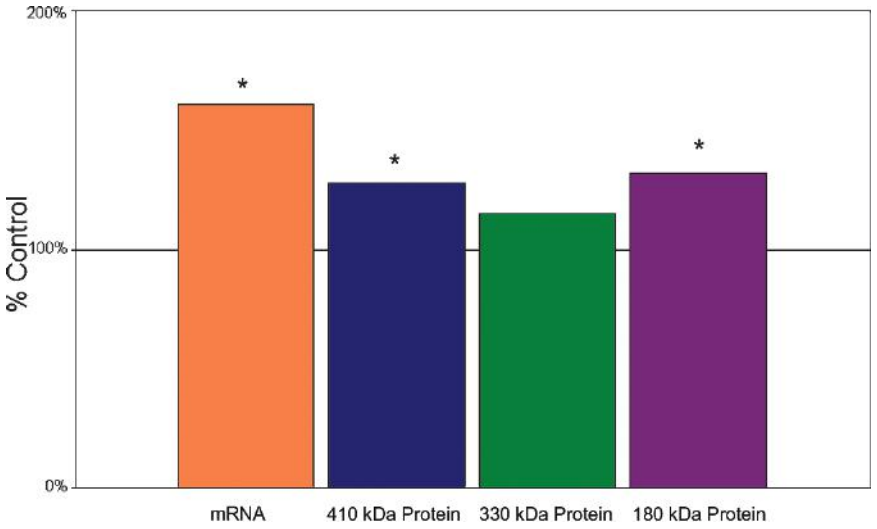

Fig. 22.6 The impact of olanzapine on rat brain levels of Reelin. Olanzapine-treated rat FC showed significant upregulation of the 410- and 180-kDa isoforms of Reelin. Reln mRNA was also significantly upregulated

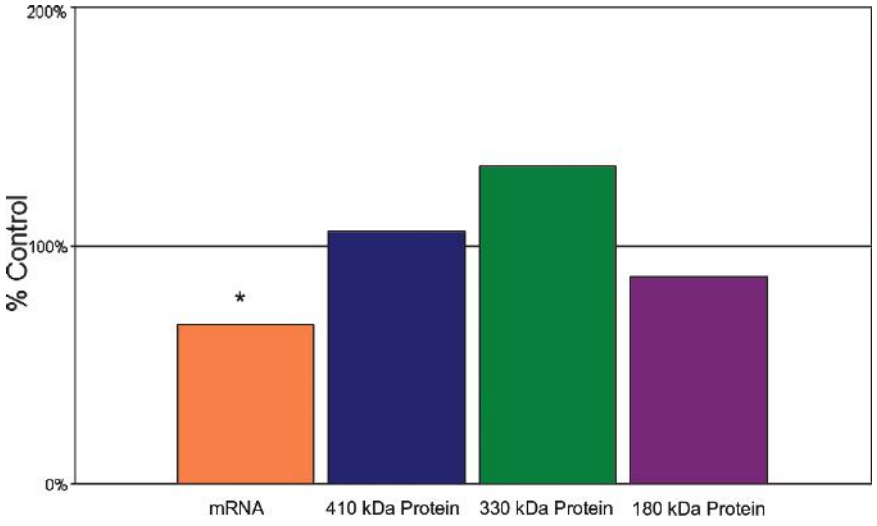

Fig. 22.7 The impact of valproic acid on rat brain levels of Reelin. Reln mRNA was significantly downregulated in rat FC as a result of treatment with VPA

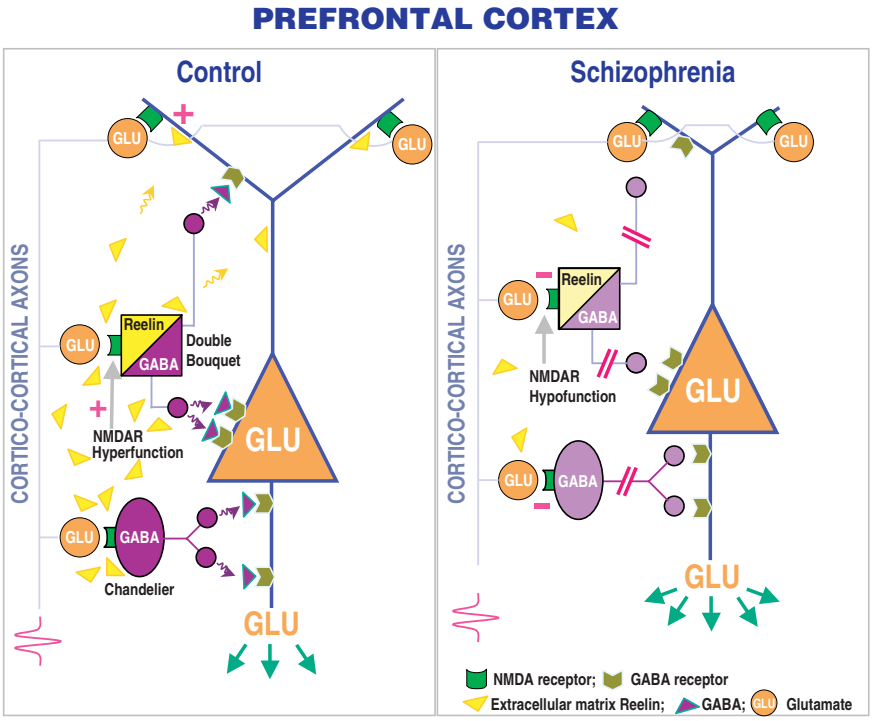

Fig. 23.1 (Control) Reelin expressed in double bouquet or horizontal cells in the upper prefrontal cortex layers is secreted by a constitutive mechanism in the extracellular matrix space and: (a) binds to the apical dendritic branches of pyramidal neurons inducing spine formation by facilitating dendritic resident mRNA translation or (b) binds to dendrites or cell bodies of GABAergic interneurons (double bouquet or chandelier cells), facilitating the action of glutamate at NMDA receptors located on GABAergic interneurons and thereby increasing the release of GABA on apical dendrites, cell bodies, and axon initial segments of pyramidal neurons.

(Schizophrenia) Reelin and GAD67 expression and reelin and GABA release are downregulated. The reelin deficit causes: (a) decreased dendritic spine density on the apical dendrites of pyramidal neurons and (b) hypofunction of NMDA receptors located on double bouquet or chandelier cells, eliciting a further decrease of GABA released on the apical dendrites, cell bodies, or axon initial segments of pyramidal neurons. The deficit of GABAergic neurotransmission results in an increased output of glutamate from the axon terminal of pyramidal neurons

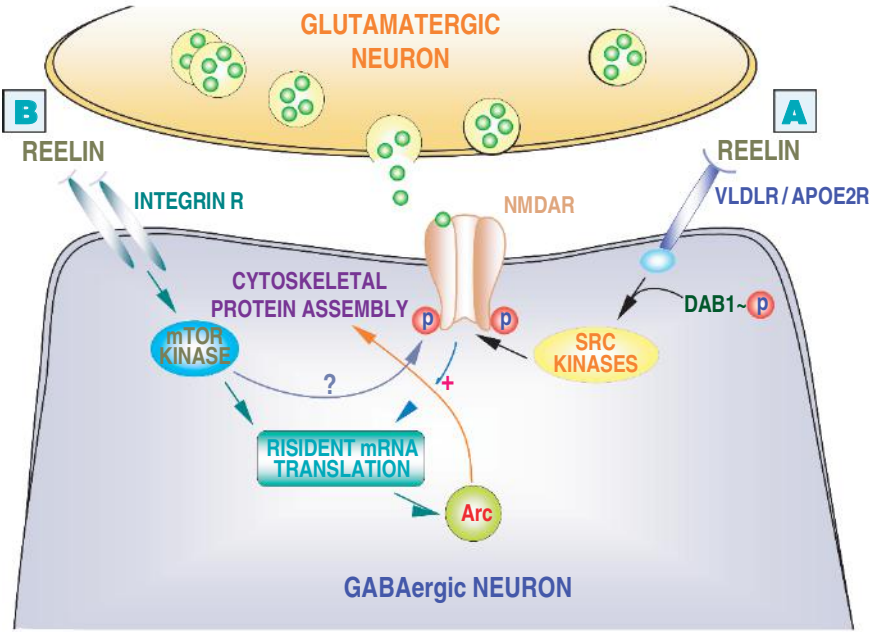

Fig. 23.2 Putative role of reelin in synaptic plasticity. Reelin is depicted binding to a dendritic postsynaptic density of a cortical GABAergic interneuron. Either (A) to VLDL or ApoE2 receptors (VLDLR or APOE2R) or (B) to integrin receptors (INTEGRINR). (A) Reelin modulates NMDA receptor (NMDAR) activity through SRC kinase-mediated tyrosine phosphorylation of the NMDAR intracellular sites (Weeber *et al*., 2002; Herz and Chen, 2006). (B) Reelin modulates Arc expression and cytoskeletal protein assembly through activation of mTOR kinase (Dong *et al*., 2003)

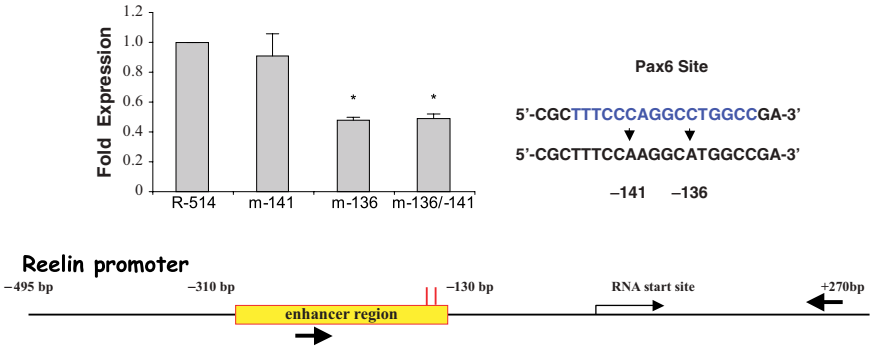

Fig. 23.6 Reelin promoter point mutations. We designed site-directed mutants within the Pax6 binding site that had previously been shown to be more heavily methylated in patients with SZ (Grayson *et al*., 2005). These corresponded to the double (–141/–136), and single promoter mutants (m –141) and (m –136). These minimal mutants were introduced into NT2 cells using transient transfection assays and reporter activity was measured 36 hr later. NT2 cells transfected with the single mutant (m –136) and double mutant construct (m –136/–141) exhibited 50% of the activity of the –514 promoter. *p, 0.05 expressed as a percent of the SV40 promoter and compared with the reelin –514 promoter for statistical purposes (one-way ANOVA followed by Fisher LSD Method)

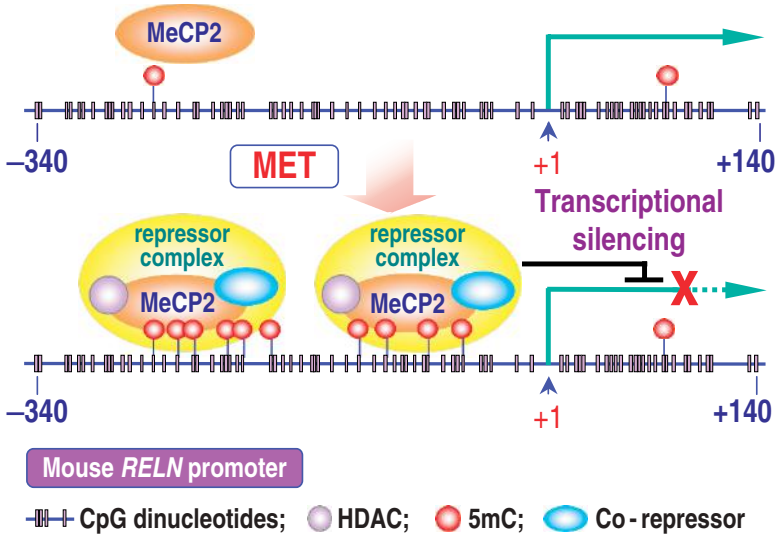

Fig. 23.7 Proposed mechanisms by which mouse *RELN* promoter hypermethylation and recruitment of chromatin remodeling complexes (MeCP2, HDACs, and co-repressors) regulate reelin gene expression. The mouse reelin (*RELN*) promoter region depicted here follows that reported by Tremolizzo *et al*. (2002) and includes the repressor protein complex. Vertical bars represent CpG dinucleotides present in this region. Pink dots denote 5mC present in the sequence. Note the increase of 5mC in MET (methionine)-treated mice. MeCP2 recruits co-repressor complexes including HDACs and induces a state of gene repression

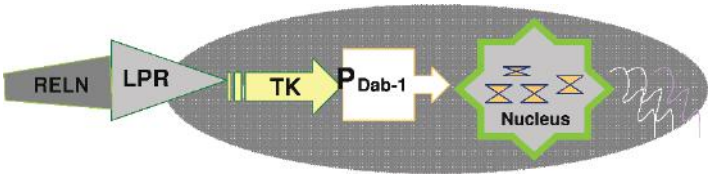

Fig. 24.1 Binding of RELN to lipoprotein receptors (LPR) activates a tyrosine kinase (TK)-dependent cascade leading to Dab1 phosphorylation and expression of several genes that lead to long-lasting structural changes

GCCCTCTG**C**GGGGCTT**TGACGTC**CCT**C**GCAGAAGAGT**C**G**C**GGGCTCAG**C**GGTC
CT**C**GACAG**C**GTCCCGTCC**C**GCTCCC**C**GG**C**GGG**C**GCCCCTCCCTGTCCTCC**C**GG
GTG**C**GAAC**C**GGG**C**GCTGGC**C**GGGGACTC**C**GGGGA**C**G**C**GTG**C**GCCCCT**C**GC**C**
G**C**G**C**GAGGTGC**C**GC**C**GAGCCAGCC**C**GAGAGGG**C**GGGGGGG**C**GGG**C**GGGG**C**G
G**C**G**C**G**C**GGGGG**C**GGGGGAG**C**GGC**C**GGGACA**C**GTGTGG**C**GG**C**G**C**GGGGGG
GA**C**G**C**GG**C**GCC**C**GGGGCTTTAAGAAGGTGTGGAG**C**GGGG**C**GGG**C**GCTTTCCC
AGGCCTGGC**C**GAGGGG**C**GT**C**G**C**GCAGAGG**C**GG**C**GG**C**GG**C**GCA**C**GGAGG**C**G
GCAGA**C**GA**C**G**C**GCTCT**C**GG**C**GCC**C**GCAGCCC**C**GGTCC**C**G**C**GCTCC**C**G**C**GGC
CCAAAGTAACTTTGGGAGC**C**GC**C**GTCTCC**C**GCGGAAACTT-exon

Fig. 24.2 A view of *RELN* promoter sequence. *RELN* harbors a CG-rich promoter with 72 candidate cytosine (C) sites for methylation and several regulatory binding sites located in 450 base pairs upstream of the coding region. A CRE binding site is underlined in the first line and several SP1 binding sites (GGGCGG) and a consensus GC box are underlined in other locations. The boldface **C**s that are followed by G are candidates for methylation, while other Cs or unmethylated Cs will be converted to T during bisulfite treatment

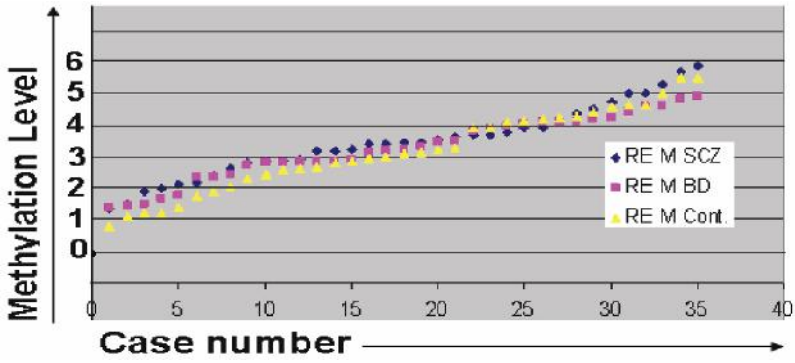

Fig. 24.4 Comparison of DNA methylation levels by qMSP, revealing that the degree of *RELN* methylation in SCZ and BD is almost twice that of the controls. To visualize the differential levels of *RELN* promoter methylation in the patients and controls, the ΔC_T of methylated product for *RELN*, normalized with the C_T of β-actin, was sorted from minimum to maximum. Thus, the increase in the percent of methylation would be exponential. As shown, the base level of *RELN* promoter DNA methylation was greater in SCZ and BD compared to the control subjects (almost twofold). This difference remained nearly the same across the entire samples; however, patients with BD showed a lesser degree of *RELN* methylation in the last part of the curve, where the level of methylation was relatively high

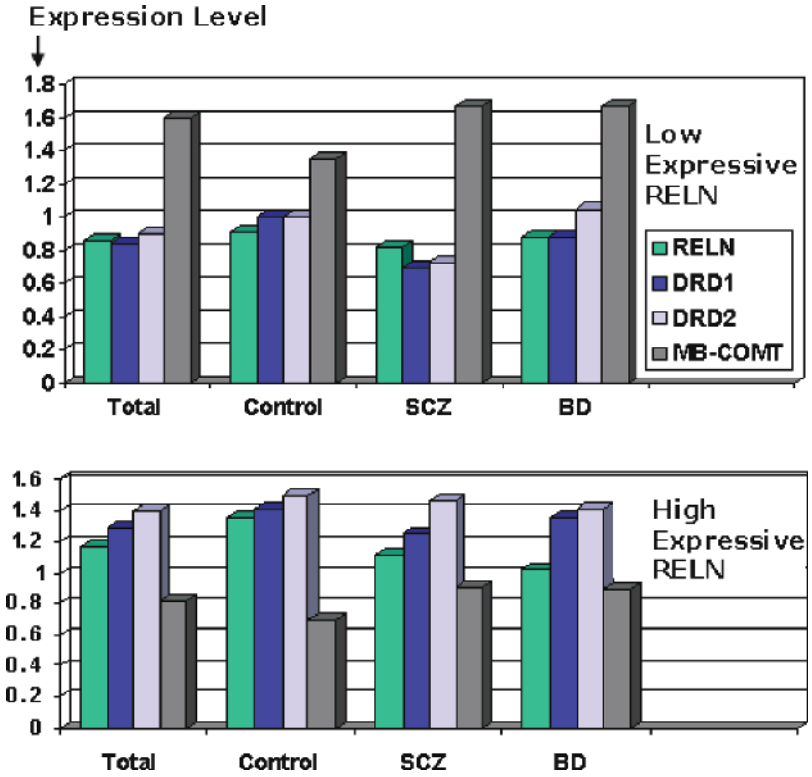

Fig. 24.5 Inverse correlation between the expression of *RELN* and *DRD1*, *DRD2*, and *MB-COMT*. Consistent with the promoter methylation status, expressions of *RELN, DRD1,* and *DRD2* appear to be correlated, but are inversely correlated with the *MB-COMT* expression in both controls and the patients, as well as in total samples. As a result, *RELN* hypoexpression could be associated with hypoactivity of dopaminergic neurotransmission in the frontal lobe

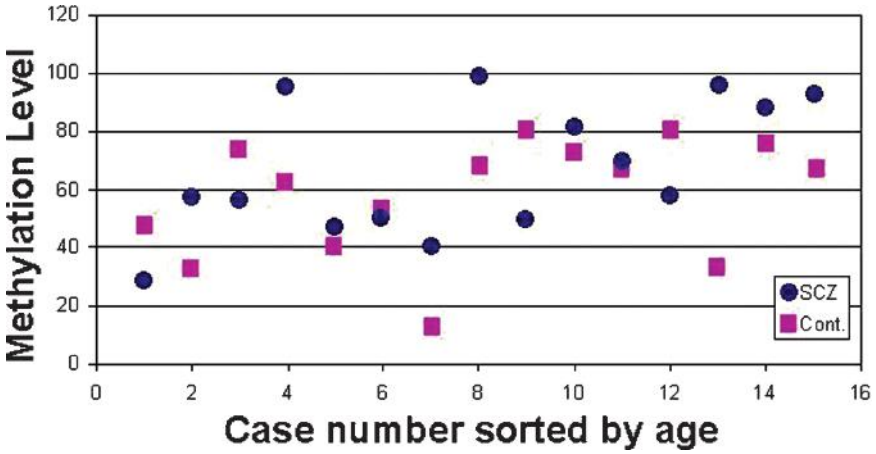

Fig. 24.6 Age-dependent increase in *RELN* promoter methylation. The degree of *RELN* promoter methylation (*Y* axis), extracted from Grayson *et al*. (2005, supplementary Table 2), was sorted by age (*X* axis). As shown, the degree of promoter methylation increased by age in both SCZ and the control subjects

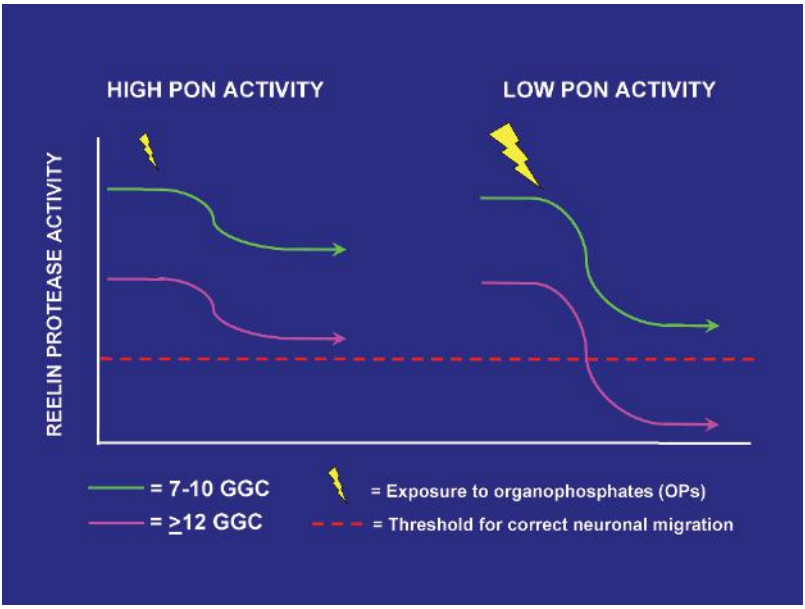

Fig. 25.2 Putative gene–environment interaction model involving the Reelin and PON1 genes, and prenatal exposure to organophosphates (OPs). Reelin gene variants genetically determine normal or reduced levels of Reelin, associated with normal or "long" GGC alleles, respectively. Both conditions are compatible with normal neurodevelopment, but prenatal exposure to OPs can transiently inhibit Reelin's proteolytic activity, which may or may not fall below the threshold critical to neuronal migration, also depending on baseline levels of Reelin. Furthermore, exposure to identical doses of OPs can affect Reelin to a different extent, depending on the amount and affinity spectrum of the OP-inactivating enzyme paraoxonase produced by the *PON1* gene alleles carried by each subject (Gaita and Persico, 2006; Persico and Bourgeron, 2006). (Modified from *Trends Neurosci*., Vol. 29, Persico, A.M., and Bourgeron, T., Searching for ways out of the autism maze: genetic, epigenetic and environmental clues, pages 349–358, copyright 2006, with permission from Elsevier)

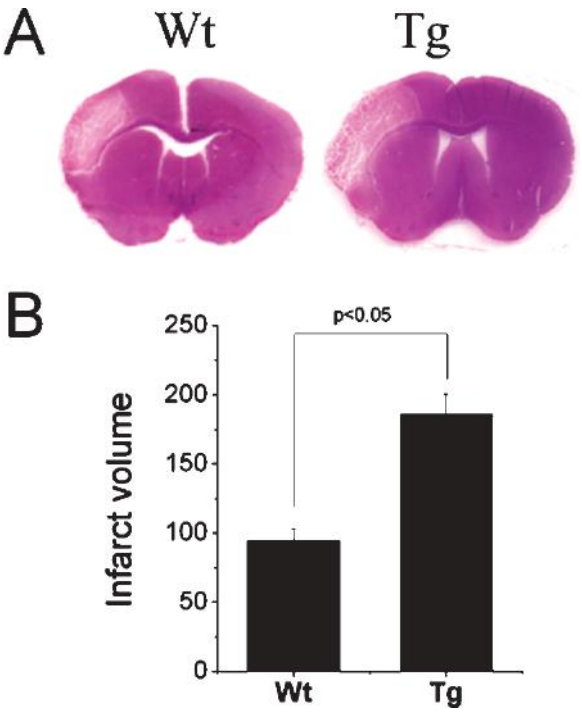

Fig. 27.1 Ischemic brain injury in wild-type (Wt) and transgenic mice with Reln deficiency (Tg) following focal cerebral ischemia. (**A**) HE staining shows an increased area of ischemic injury in *reeler* mice compared to WT mice. (**B**) Quantification of infarct volume in WT and *reeler* mice. $p<0.05$ compared to WT (Student's *t*-test)

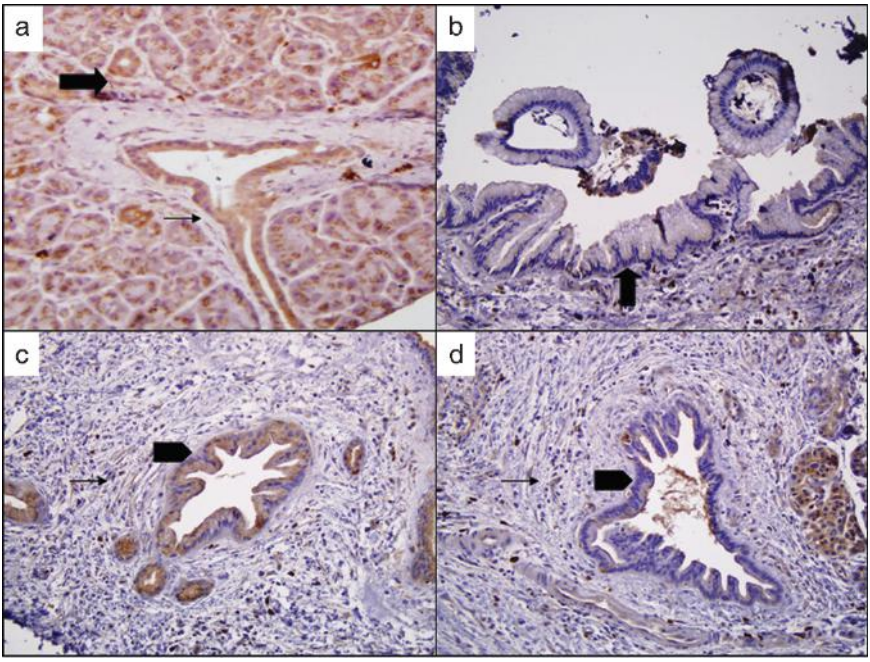

Fig. 28.1 Immunohistochemical analysis of RELN in normal pancreas (**a**) and IPMN (**b**) and PanIN lesions (**c**,**d**). The thin arrow in **a** is pointing to pancreatic ductal epithelium, while the thick arrow is pointing to pancreatic acinar cells. In **b**, the arrow is pointing to the abnormal ductal epithelium of an IPMN; in **c** and **d**, the thick arrowhead is pointing to the abnormal ductal epithelium of a PanIN. The thin arrow in **c** and **d** is pointing to the surrounding fibrosis